

Spatial asymmetries in ELM induced pedestal density collapse in ASDEX Upgrade H-modes

I. Nunes¹, M. Manso¹, F. Serra¹, L. D. Horton², G. D. Conway², A. Loarte³ and the ASDEX Upgrade and CFN Reflectometry Teams

¹Associação EURATOM-IST Centro de Fusão Nuclear, IST, 1049-001 Lisboa - Portugal

²Max-Planck Institut für Plasmaphysik, EURATOM-Association IPP, Garching D-85748, Germany

³EFDA CSU Garching, Garching D-85748, Germany

1. Introduction

Edge localized modes (ELMs) cause a repetitive loss of plasma edge confinement leading to a fast (few hundreds of μs) transport of particles and energy from the main plasma to the scrape-off layer. In next step devices this may lead to periodic large power loads to the divertor and main wall causing erosion and/or melting of the plasma facing components, limiting their lifetime.

This paper reports results on measurements of the electron density profiles, obtained with a broadband microwave reflectometer installed at ASDEX Upgrade. This reflectometry system measures the electron density profiles n_e simultaneously at the low-field (LFS) and high-field side (HFS) mid-plane with high temporal (35 μs) and spatial (5mm) resolution. It operates in O-mode, in the range of frequencies from 16 to 100 GHz at the LFS and 16 to 72 GHz at the HFS, probing the midplane over a density range of $[0.30-10]\times 10^{19}\text{m}^{-3}$ at the LFS and $[0.30-6.64]\times 10^{19}\text{m}^{-3}$ at the HFS [1]. The typical sweep rate is 25 μs with a minimum repetition period of 35 μs which allows the characterization of several entire ELM cycles (with typical frequencies between 20 and 130 Hz).

Previous results from ASDEX Upgrade [2] show that, qualitatively, the electron density profile perturbation caused by an ELM is similar at both high-field (HFS) and low-field (LFS) side and that the collapse of the density pedestal occurs first at the LFS and later at the HFS. Here we report a study of the radial extent of the ELM perturbation on both HFS and LFS and its average radial velocity.

2. Density Collapse

The ELM events show, typically, the same dynamics in the edge density profiles: prior to the onset of the ELM, an increase of the density fluctuations in the entire density profile is observed. At the onset, the density fluctuations increase further and the reflectometry signals become so highly perturbed that the reconstruction of the density profiles during this interval of enhanced MHD is not meaningful for $\sim 200 \mu\text{s}$. The collapse of the density profiles is observed to occur first at the LFS and later at the HFS, which may be explained by the propagation of the perturbation from the LFS to the HFS consistent with a ballooning character of the ELM. The time lag ($\Delta t_{\text{LFS/HFS}}$) between the collapses of the density at both sides is inferred from the sudden increase of fluctuations on the group delay signals. This delay is found to be comparable with the ion parallel transport time (τ_{\parallel}) with the main dependence being on the connection length [2], as shown in figure 1.

3. ELM affected depth

The radial extent of the ELM perturbation (ELM affected depth) of the density profiles within the region of closed flux lines can be determined by simply using the density profile before the ELM and the collapsed density profile after the ELM. The ELM affected depth is then

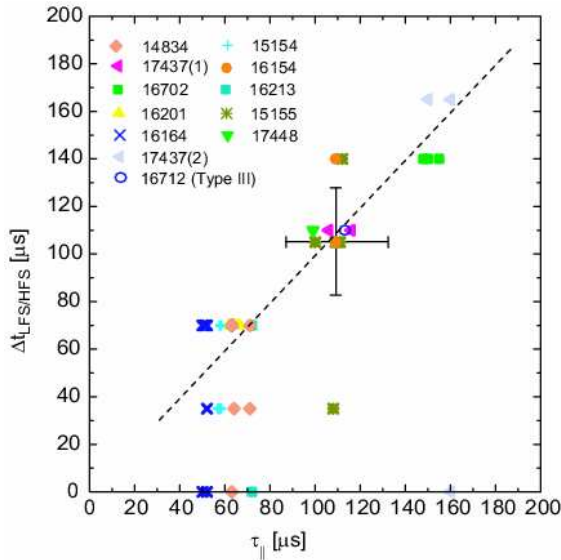


Figure 1 – Time lag between the collapse of the pedestal density at the HFS and LFS

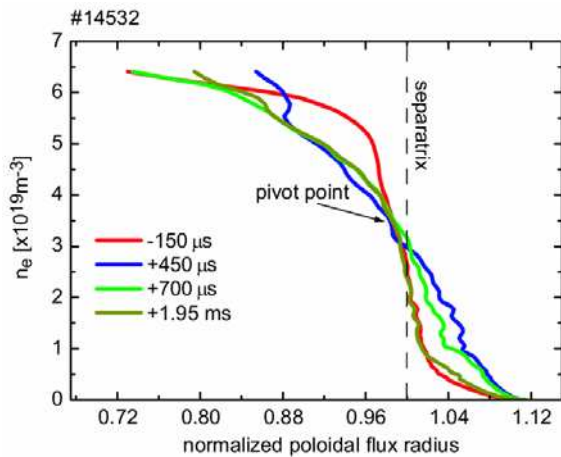


Figure 2 – Time evolution of the density profile before and after the ELM. A pivot point (inside the separatrix) is observed.

affected depth is correlated with the ELM particle losses [2] with smaller affected depths being associated with smaller ELM particle losses. The ELM affected depth was also determined for the HFS (figure 3 – open symbols), and it is similar to that at the LFS for similar pedestal density in real space (although in flux coordinates this affected depth is smaller).

4. Radial velocity

An ELM event causes the collapse of the density pedestal and a broadening of the density profiles in the scrape-off layer (SOL), as shown in figure 2. The radial velocity (v_r) for a fixed density layer is defined by the ratio of the radial displacement of that density layer (with respect to its previous position) to the time interval for this displacement. This velocity, thus,

given by the distance between the pivot point and the inner radial point where no change of the density reflected layer is observed as shown in figure 2. Figure 3 shows that the ELM affected depth (normalised to the plasma minor radius) at the LFS decreases slightly with the pedestal density (normalised to the Greenwald density), but does not show a clear dependence on the plasma parameters varied here (I_p , δ , P_{IN}) for the range of pedestal density investigated ($n_{e,ped} < 7 \times 10^{19} m^{-3}$). The ELM perturbation affects the outermost 10-20 cm (20-40% of the plasma minor radius), which is similar to the observations in JET [4], DIII-D [5] and JT-60U [6]. Furthermore, the ASDEX Upgrade data show that the ELM

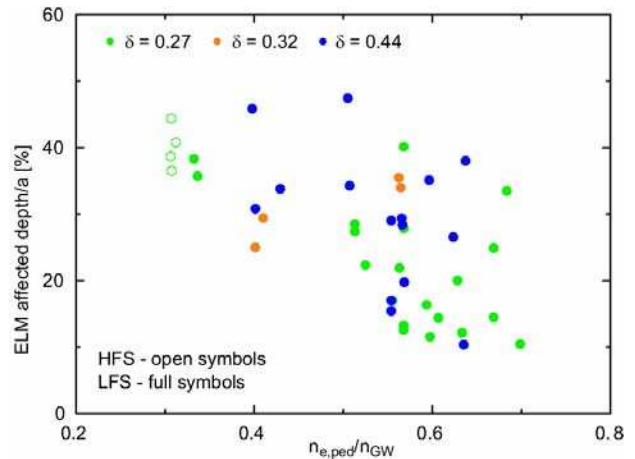


Figure 3 – HFS and LFS ELM affected depth normalised to the plasma minor radius.

corresponds to that of the radial propagation of particles under the assumption that this propagation is mostly convective and occurs in much shorter timescales than those associated with radial diffusion. If that were not the case, diffusion could lead a significant decrease of the plasma density in the layer as it propagates inwards and outwards after the ELM, which would lead to an underestimate of the radial propagation velocity of the particles expelled by the ELMs, particularly at large distances from the separatrix. Typical effective diffusive velocities in the SOL/pedestal region in ASDEX Upgrade Type I ELMy H-modes are $\sim 10\text{--}30$ m/s [7], which are a factor of 2 – 5 smaller than the value of v_r determined with this technique (see below), thus justifying a posteriori the validity of the assumptions required for its derivation.

The minimum time interval used in this

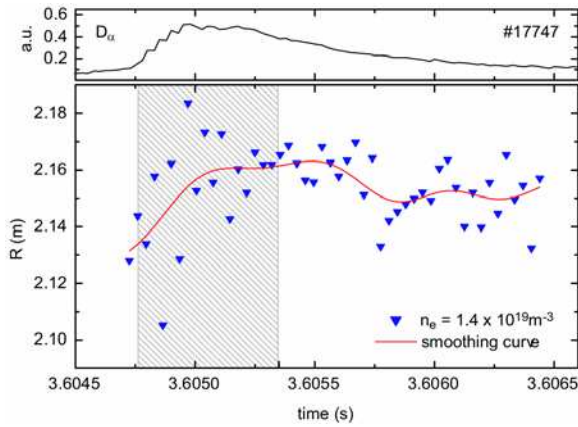


Figure 4 – Time evolution of the radial position of the $n_e = 1.4 \times 10^{19} \text{ m}^{-3}$ layer (in the SOL). Note that the pivot point density is $\sim 3.4 \times 10^{19} \text{ m}^{-3}$.

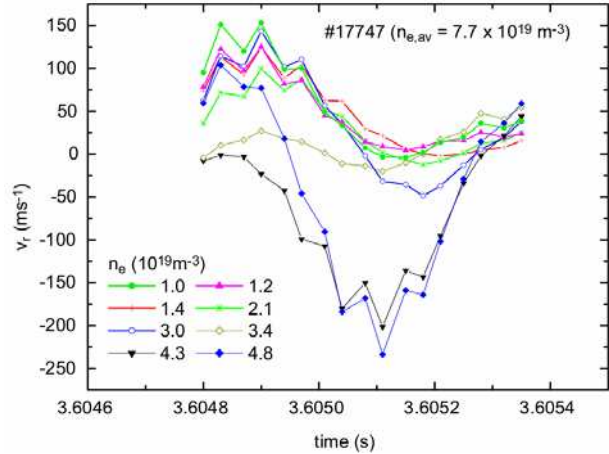


Figure 5 – Radial velocity of several density layers as a function of time for a discharge with $I_p = 0.8$ MA, $B_T = 2T$ and $n_{e,av} = 7.7 \times 10^{19} \text{ m}^{-3}$.

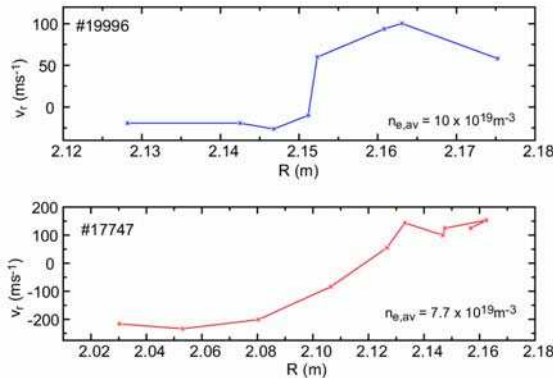


Figure 6– Maximum radial velocity as a function of major radius for two discharges (a) $I_p = 1.0$, $B_T = 2T$ $n_{e,av} = 10 \times 10^{19} \text{ m}^{-3}$ and (b) $I_p = 0.8$ MA, $B_T = 2T$ and $n_{e,av} = 7.7 \times 10^{19} \text{ m}^{-3}$.

the first profile used to determine v_r is taken approximately $200 \mu\text{s}$ after the ELM onset. Figure 5 shows the time evolution of v_r for several density layers outside and inside the pivot point ($\sim 3.4 \times 10^{19} \text{ m}^{-3}$). In the SOL and far from the pivot point, v_r is typically $\sim 150 \text{ ms}^{-1}$ while inside the pivot point the radial velocity is $\sim -200 - -250 \text{ ms}^{-1}$. Figure 5 is a typical example: v_r inside and outside the pivot point may be different, as well as the time evolution of the velocity for each density layer. In the initial phases ($\sim 200 - 300 \mu\text{s}$ after the ELM), the layers propagate at maximum velocity in the SOL, finally coming to a stop after an additional 300

analysis is defined by the temporal resolution of the reflectometer ($35 \mu\text{s}$). The density profile immediately before the onset of the ELM is used as a reference for the initial position of the various density layers whose movement is studied. The time evolution of the position of a density layer in the SOL is shown in figure 4. The radial velocity is calculated using smoothed values of the above

quantity (also in figure 4). The error in the measurements is approximately $\pm 25 \text{ ms}^{-1}$. Due to the strong MHD activity during the ELM and its influence on the reflectometry signals,

μs (i.e., 600 μs after the ELM). This deceleration can be due either to a slowing down of the propagation itself in time or to losses of particles to the divertor along the field line. On the contrary, the inwards movement of the density maximum reaches its maximum speed at later times compared to the SOL propagation ($\sim 600 \mu\text{s}$ after the ELM), indicating that the dynamics of inwards and outwards propagation from the pivot point are different. Typically at the time of maximum velocity of the layers in the SOL ($\sim 200 - 300 \mu\text{s}$ after the ELM), v_r is approximately constant for all density

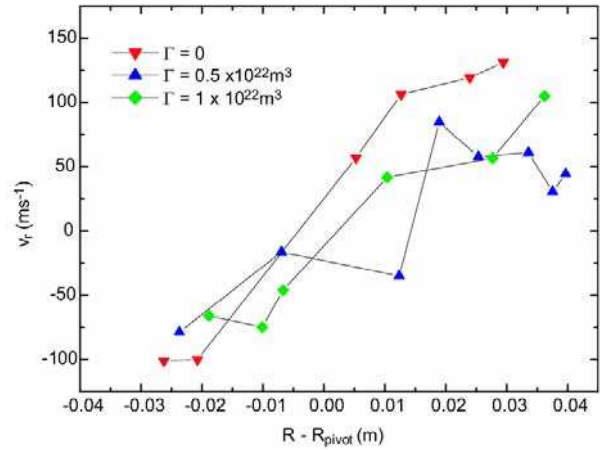


Figure 7 – Maximum radial velocity as a function of major radius for a density scan with $I_p = 1.0$, $B_T = 2T$.

layers (far from the pivot point) both in the SOL and inside the pivot point, as shown in figure 6 where the maximum v_r for each density layer is plotted against the major radius.

In order to determine the physics mechanisms behind the radial propagation of particle during the ELM, the radial velocity has been determined for a 3-point gas fuelling (Γ) scan in plasmas with $I_p = 0.8 \text{ MA}$, $B_T = 2T$ in Type I ELMy H-mode. Figure 7 shows the maximum v_r for several density layers inside and outside the pivot point for these three discharges. A decrease of v_r at the SOL (from 125 ms^{-1} to 50 ms^{-1}) of about a factor of 2 is observed with increasing gas fuelling rate, indicating a possible correlation of v_r with ELM size and ion parallel transport time as suggested in [8], but further analysis is needed. These values have similar order of magnitude to those determined for JET [8, 9].

5. Summary

The comparison between HFS and LFS density profiles during an ELM event shows a time delay between the collapses of the density comparable with the ion parallel transport time. The radial extent of this perturbation is similar at the HFS and LFS in real space and extends over $\sim 20\text{-}40\%$ of the minor plasma radius. The radial velocity of the perturbation in the SOL is $\sim 125\text{-}150 \text{ ms}^{-1}$ (at the lowest densities and decreases with fuelling rate (and pedestal density) by approximately a factor of 2 for otherwise constant plasma parameters.

Acknowledgments

This work has been carried out in the frame of the Contract of Association between the European Atomic Energy Community and Instituto Superior Técnico (IST) and of the Contract of Associated Laboratory between Fundação para a Ciência e Tecnologia (FCT) and IST. The content of the publication is the sole responsibility of the authors and it does not necessarily represent the views of the Commission of the European Union or FCT or their services.

References

- [1] Silva A. et al., Rev. Sci. Instrum. 67, (1996), 4138; [2] Nunes I. et al, Nuclear Fusion, 44, (2004), 883; [4] Loarte A. et al., Plasma Phys. Control. Fusion 44 (2002) 1815; [5] Leonard A. et al., Plasma Phys. Control. Fusion 44 (2002) 945; [6] Chankin A. et al., Nucl. Fusion 42 (2002) 733; [7] Kim, J.W. et al, Jour. Nuc. Mat. 290-293 (2001) 644; [8] Gonçalves B. et al., Plasma Phys. Control. Fusion, 45 (2003) 1627; [9] Fundamenski W. et al., Nucl. Fusion 44 (2004) 20